Submitted to J. of Material Sciences

UCRL-19086 Rev.
Preprint

c. 2

ON CONTINUUM MODELS OF DUCTILE FRACTURE

William W. Gerberich

December 1969

AEC Contract No. W-7405-eng-48

LAWRENCE RADIATION LABORATORY
UNIVERSITY of CALIFORNIA BERKELEY

UCRL-19086 Rev.

25

DISCLAIMER

UCRL-19086 Rev.

ON CONTINUUM MODELS OF DUCTILE FRACTURE

William W. Gerberich

Inorganic Materials Research Division, Lawrence Radiation Laboratory, and Department of Materials Science and Engineering, College of Engineering, University of California
Berkeley, California

December, 1969

ABSTRACT

Several fracture criteria are reviewed with respect to ductile fracture. It is suggested that both critical crack-tip displacement, $2V_c^*$, and critical fracture strain, ε^*, criteria may describe the fracture of a ductile second phase rod in a ductile matrix. As a first approximation, this is experimentally verified by observations of ductile stainless steel fibers fracturing in an age-hardened aluminum matrix. For 0.05, 0.10 and 0.20 volume fraction composites, the average fracture strains are calculated to be 1.15 as compared to a measured average of 0.93 while the average critical crack-tip displacement is calculated to be 0.50 mm. as compared to an "observed" average of 0.40 mm. The statistical variation in the fracture strain was not sufficiently small to allow any choice between these proposed criteria. In fact, both the experimental and theoretical evidence point to the equivalency of these criteria as given by

$$2V_c^* = \pi \ell^* \varepsilon^*$$

where ℓ^* is the microstructural unit in front of the crack over which the strain is greater than or equal to ε^*.

1. INTRODUCTION

Many continuum approaches to fracture have been developed in the last twenty years including stress concentration, stress intensity and strain energy release rate (modified Griffith) concepts. However, there has been limited use of these in the understanding of how to make materials more resistant to fracture. For this reason, one of the most promising areas is that of applying continuum mechanic and continuous dislocation distribution theory to the vicinity of the crack, in the region where the microstructural constituents control fracture nucleation and growth. Two such developments are the crack-tip displacement concepts as espoused by Cottrell [1], Wells [2] and Tetelman and McEvily [3] and the ductile fracture concepts of McClintock, et al. [4,5]. The former describes the fracture process in terms of a "micro-tensile" sample fracturing at the crack tip while the latter describes ductile shear fracture in terms of a hole-coalescence theory.

It is the purpose of this paper, first, to develop in a very simple way some of the current ductile-fracture concepts and then attempt to test these concepts using some experimental evidence obtained from crack propagation studies of a fiber reinforced composite. A composite system was used so that the unit over which fracture took place would be unambiguous and so that the flow and fracture characteristics of the individual components could be characterized. All of these values are necessary but not readily attainable in the study of homogeneous materials. Therefore, the composite system was utilized so that various ductile fracture criteria could be properly assessed. The experimental study includes the detection of the fracture history of stainless-steel fibers in an aluminum matrix by an acoustic emission technique; metallographic analysis of fracture strains involved in fiber fracture; and

stress-intensity analysis of crack-propagation characteristics.

2. THEORETICAL BACKGROUND

Many contemporary fracture concepts have their roots based in the energy balance concept originally derived by Griffith [6] to explain fracture phenomena in glass. He assumed that spontaneous fracture would occur when the total energy of the system was unchanged by small variations of the crack length, i.e.

$$\frac{\partial(U + V)}{\partial C} = 0 \tag{1}$$

where U is the change in the strain energy of the system with a flaw, V is the potential energy of creating new fracture surfaces and 2C is the major axis of an elliptical crack. For essentially brittle materials such as glass, the energy associated with creating new surfaces is the surface tension, γ_s. Without stating the details, which have been reiterated many times elsewhere, e.g., [3, 7] equation (1) leads to

$$\sigma = \left[\frac{2E\gamma_s}{\pi C}\right]^{1/2} \tag{2}$$

where σ is the applied stress and E is the tensile modulus of elasticity. For materials that do not behave elastically or have atomically sharp cracks, it is appropriate to modify equation (2). First consider the crack-tip radius effect. Tetelman and Johnston [8] have interpreted Orowan's [9] analysis to show that

$$\sigma = \left[\frac{2E\gamma_s}{\pi C} \cdot \frac{\rho}{a_0}\right]^{1/2} \tag{3}$$

where ρ is the crack-tip radius and a_0 is the atomic spacing. Although the justification of equation (3) for plastically deforming materials might be argued on theoretical grounds, it nevertheless gives a useful qualitative interpretation of the crack-tip radius effect. If some

mechanism such as chemical dissolution blunts the crack tip, the stress which can be maintained prior to catastrophic fracture increases. Next, consider inelastic behavior. Orowan [9] and Irwin [10] interpreted Griffith's equation for metals in terms of the plastic energy absorption, γ_p, occurring during crack extension. Instead of γ_s controlling, there is a combined term, $\gamma_m = \gamma_s + \gamma_p$, which is substituted in equation (2) for γ_s. In the notation of Irwin who defines the critical parameter as the strain energy release rate, G,

$$G = 2\gamma_m = \frac{\sigma^2 \pi C}{E} \tag{4}$$

Combining equations (3) and (4), it is seen that

$$G = 2\gamma_s \frac{\rho}{a_0} \tag{5}$$

which indicates that the actual value controlling fracture increases with ρ/a_0. As this interpretation is based upon an extension of elastic analyses, it would seem to be quantitatively suspect when $\rho >> a_0$ (e.g. $10^4 a_0$) which is the case for many reasonably tough materials.

A second approach which may have more applicability to ductile fracture is the crack-tip displacement concept. It has been proposed [1, 3] that slow crack growth advances by the fracturing of "micro-tensile" samples at the crack tip. The length of the sample is limited by the root radius of the crack and the width is limited by those microstructural factors which limit ductility. Since the gage length of the sample would be nearly equal to the diameter of the crack tip, 2ρ, then the crack-tip displacement is given by

$$2v_c = 2\rho\varepsilon \tag{6}$$

where ε is the strain adjacent to the crack front. This, then, leads to a failure criterion [1, 3] when the strain reaches the fracture ductility,

ε^*,

$$2v_c^* = 2\rho\varepsilon^* \tag{7}$$

Taking the fracture strain to be exceeded over the dimensions of the micro-tensile sample, one can easily visualize a brittle second phase rod fracturing ahead of the main crack. Alternatively, a ductile rod at the crack tip could be visualized to neck down considerably prior to fracture. For applied stresses up to about 60 percent of the yield strength, σ_{ys}, the crack-tip displacement is given by [11]

$$2v_c = \frac{\pi\sigma^2 c}{\sigma_{ys} E} \tag{8}$$

From equations (4) and (8), it is seen that

$$2v_c = \frac{G}{\sigma_{ys}} \tag{9}$$

which demonstrates the relationship between crack-tip displacement and the strain energy release rate. Consider this with respect to the point of fracture. If one stretches the applicability of the Griffith approach and the crack-tip displacement approach to a single system, then combining equations (5), (7) and(9) and eliminating ρ gives

$$\gamma_s = \sigma_{ys}\varepsilon^* a_0 \tag{10}$$

The physical interpretation of this is that in truly brittle materials if the yield strength reaches the theoretical strength of the solid and the fracture strain is exceeded only over the atomic spacing, then $\varepsilon^* a_0$ is equivalent to the crack-tip displacement, i.e. the strain times the gage length. It is obvious then that equations (5) and (7) are not compatible if sufficient microyielding occurs prior to fracture. This has been pointed out by Tetelman and McEvily [3] who relegate equation (5) to those systems where continuous cleavage may proceed with stresses at

the crack tip at the theoretical limit.

Cottrell [1] has generalized the crack tip displacement concept in terms of the work of fracture per unit fracture area. In terms of the displacement, $2v_c$, and stress, σ_c, at the crack tip, the work is given by

$$2\gamma = 2\int_0^{\infty} \sigma_c \, dv \tag{11}$$

Cottrell proposed a rectilinear approximation to the law of force so that at fracture, equation (11) becomes

$$2\gamma = 2\sigma_c v_c^* \tag{12}$$

For elastic behavior, $2v_c^*$ is the atomic dimension and the stress at the crack tip, σ_c, is the theoretical strength or about E/5, giving

$$\gamma_s = 0.1\, Ea_0 \tag{12a}$$

which is in reasonable agreement with measured values of γ_s. For plastic behavior, $2v_c^*$ is related to the crack-tip radius and fracture strain by equation (7) and σ_c is the yield strength, giving

$$2\gamma_m = G = \sigma_{ys} \cdot 2v_c^* = 2\sigma_{ys}\rho\varepsilon^* \tag{12b}$$

Physically, this demonstrates that the larger the critical crack-tip displacement and, as a result, the larger the crack-tip radius and fracture strain that can be sustained prior to catastrophic failure, the larger the energy absorption.

A criticism of either the energy or crack-tip displacement approaches can be made in that there has been no explicit microstructural size factor involved in any of the equations proposed thus far. For example, what are the relative contributions of large particles with good ductility as opposed to small particles with poor ductility. In order to make an unambiguous comparison, simultaneous consideration of both size and

ductility effects is needed. McClintock, et al. [4,5] have taken such a detailed approach for ductile fracture by a hole-growth mechanism. In a more general way, McClintock and Irwin [2] have derived the criterion for fracture under anti-plane strain behavior to be

$$K_{IIIC} = \tau_{ys} [\pi \ell^* \xi^* / \xi_y]^{1/2} \tag{13}$$

where τ_{ys} is the shear yield strength; ξ^* is the shear strain at fracture; ξ_y is the elastic shear strain; ℓ^* is the microstructural unit over which the fracture strain is exceeded; and K_{IIIC} is the critical value of the mode III stress intensity factor related to strain energy release rate, G_{III}, and shear modulus, μ, by

$$K_{III} = [2\mu G_{III}]^{1/2} \tag{13a}$$

It is seen that there is some microstructural unit, ℓ^*, over which the fracture strain is exceeded, causing crack growth to occur at the condition, K_{IIIC}.

Similarly, a tensile fracture criterion can be made by using analagous strain distributions, stresses and strains. Gerberich [13] has demonstrated that the analogy to the mode III strain distribution also approximates that for a crack under tensile loading, giving

$$\varepsilon_1 = \frac{\sigma_{ys} R_p}{E\ell} \tag{14}$$

where ε_1 is the maximum principal strain, R_p is the plastic zone diameter and ℓ is the distance in front of the crack tip. McClintock [14] has suggested that R_p be given in terms of the mode I stress intensity factor by

$$R_p = \frac{K_I^2}{\pi \sigma_{ys}^2} \tag{15}$$

where K_I is related to the mode I strain energy rate† by

$$K_I = [EG_I]^{1/2} \tag{15a}$$

Again, assuming that the fracture strain is exceeded over ℓ^* so that $\varepsilon_1 \geq \varepsilon^*$, a combination of equations (14) and (15) give

$$K_{IC} = [\pi \sigma_{ys} E \ell^* \varepsilon^*]^{1/2} \tag{16}$$

This failure criterion is schematically shown for a ductile rod in fig. 1. It is now useful to consider how these concepts might apply to the observations made on a unidirectional composite where the "microstructural" size and ductility factors are known.

3. EXPERIMENTAL APPROACH

In order to test a ductile fracture criterion, it was necessary to have both a ductile matrix and fiber so that relative strength and ductility characteristics could be evaluated.

3.1 Material Selection

One such material system consists of ductile steel fibers in aluminum where diffusion bonding does not significantly degrade the mechanical properties of the fibers. As such a composite could be purchased commercially, 2.54 mm. thick plates with volume fractions of 0.05, 0.10, 0.20 and 0.40 were obtained.†† The particular

---

† This is for plane stress conditions. For plane strain considerations, the right hand side of equation (15a) must be multiplied by $(\frac{1}{1-\nu^2})^{1/2}$, where ν is Poisson's ratio.

†† Harvey Aluminum Company, Torrance, California

composites evaluated were made up of the following constituents:

(wt.%)	C	Mo	Ni	Cr	Mn	Si	Fe	Cu	Zn	Mg
N355 stainless steel (0.23 mm. diameter	0.13	2.85	4.5	15.5	0.75	0.35	bal.			
2024-T4 aluminum				0.1	0.6	0.5	0.5	4.4	0.25	1.5

Preparation of the composites was essentially by hot-pressing layups at about 500°C in a 1000 ton hydraulic press. Afterwards, the aluminum was aged to the T4 condition. Cross sections of three volume fractions are shown in fig. 2. It is seen that a relatively uniform spacing of fibers was attained with little void content in the matrix.

3.2 Technique for Measuring Stress Intensity

Single-edge notch specimens were utilized to study a crack growing across the fibers. A crack-line loaded sample was chosen since this provides about a 10:1 mechanical advantage with respect to failing the specimen in uniaxial tension. For this reason, there is no danger of failing the specimen at the loading pin holes. The specimen configuration, which was essentially 51 mm. wide by 76 mm. high, is indicated in fig. 3. Knowing the load (P) the specimen thickness (B) width (W) and crack length (C), the stress intensity can be determined from

$$K = \frac{P}{BW^{1/2}} \; f\left(\frac{C}{W}\right) \qquad (17)$$

where f(C/W) as given in fig. 3 is taken from the numerical solution of Srawley and Gross [15]. The height of the specimen was not always the same due to material availability, but W/Hp did stay within the limits

indicated in fig. 3. Specimens were pulled at a crosshead speed of o.1cm/min. and load-time recordings were made to maximum load, at which point specimens were unloaded for metallographic examination.

3.3 Technique for Measuring Elastic Waves

During the crack propagation tests, a technique for monitoring discontinuous crack growth was utilized. This technique is based upon the detection of elastic waves associated with the energy release of a crack jump. Detection of such stress-wave emission (SWE) as connected with discontinuous crack motion has been accomplished under conditions of rising load [16], stress-corrosion-cracking [17], and spontaneous strain-aging embrittlement [18]. Essentially, a SWE is converted to an electrical signal by a piezoelectric crystal which may be mounted directly to the specimen or be contained in an attached transducer such as an accelerometer. For the relatively large SWE expected in the present study, an accelerometer transducer was utilized as indicated schematically in fig. 4. The voltage signal from the accelerometer is amplified by the charge amplifier, filtered to cut out extraneous mechanical noises, further amplified to drive a damped galvanometer with high frequency response, and directly recorded on an oscillograph. In this way, it was anticipated that the large SWE associated with fiber fracture could be used to determine the exact load at which fiber breaks occurred.

3.4 Metallographic Technique

After the test, the fracture path was studied by sectioning the partially-cracked fracture specimens. As the specimens were unloaded somewhat after maximum load but prior to total failure, the orientation and position of the crack tip with respect to the ductile fibers was

obtained. Also possible was an estimate of the fracture ductility since the necking profile of the fractured fibers gives a measured fracture strain from

$$\varepsilon_f = \ln \frac{A_o}{A_f} \tag{18}$$

where A_o and A_f refer to original and final cross-sectional areas of the fibers. For these measurements, some of the polishing planes were not mid-thickness and care was taken to reconstruct profiles so that reasonable estimates of fracture strains could be made. Additional confirmation of the fracture strains was desired and so one 0.20 volume fraction specimen was pulled to complete fracture. The fracture surface was then examined with a JEOLCO JSM-1 scanning electron microscope operated at 25kV in the secondary electron mode.

4. RESULTS AND DISCUSSION

From the uniaxial tensile and crack-propagation data obtained on these unidirectional composites, it was possible to test the several fracture criteria under discussion.

4.1 Uniaxial Behavior

Mechanical properties of the individual constituents are given in the following tabulation:

	Modulus of Elasticity (kg/mm^2)	Poisson's Ratio	Yield Strength (kg/mm^2)	Ultimate Strength (kg/mm^2)
Stainless Steel Fibers	21×10^3	~ 0.3	302	315
2024-T Aluminum	7.3×10^3	0.33	35	47.5

The stainless steel results represent the average of 10 fibers extracted from 0.10 and 0.20 volume fractions while the aluminum data are nominal values taken from the literature. The ultimate tensile strength data conformed to a rule

of mixtures, which, in terms of a perfectly elastic-plastic matrix, is given by

$$\sigma_{comp} = \sigma_{m_{ys}} V_m + \sigma_f V_f \qquad (19)$$

where σ are stresses, V are volume fractions, m and f denote fiber and matrix, and ys denotes yield strength. However, if some strain-hardening in the matrix occurs and the total plastic strain at fracture is considerable, then a closer estimate might be

$$\sigma_{comp} = \sigma_{m_{UTS}} V_m + \sigma_f V_f \qquad (20)$$

where UTS denotes ultimate tensile strength. These two relationships are seen to represent the lower and upper bounds for the observed behavior in fig. 5.

4.2. Fracture Behavior

The answers to two questions were necessary if any description of the fracture process were to be meaningful with respect to establishing a failure criterion. First, the load and crack length associated with each fiber fracture were needed so that a stress intensity level could be determined for each fiber break. Secondly, it was necessary to know the position of the advancing crack with respect to the fiber break and the critical fracture strain involved in that fiber break. The first question was answered using the acoustic emission technique while the second was investigated via metallography and scanning electron microscopy.

SWE Observations

Monitoring the crack propagation tests with the acoustic emission technique allowed pin-pointing of the fiber breaks. Two examples of the SWE associated with crack propagation across steel and boron fibers in

metal-matrix composites are shown in fig. 6.† Noting the slight differences in time scale, there are at least an order of magnitude more SWE emanating from the fracture of boron fibers. Although this is partly due to the fact that there were about twice as many boron fibers per unit fracture area, it can mostly be attributed to multiple breaks (5-10 typically) in the boron fibers as compared to single breaks in the steel ones.

Further correlation of SWE to stainless-steel fiber fracture was obtained by comparing the load drops occurring during fiber fracture to the stress waves. As noted in fig. 7, each load drop was coincident with the occurrence of a large SWE. In some instances, two SWE occurred almost simultaneously which indicated two fibers fracturing even though the load only dropped once. For two 10 percent volume fraction specimens, metallographic sectioning indicated a total of 54 fractured fibers while SWE observations indicated a total of 52. The excellent correlation between these emitted waves and the fiber fracture allowed determination of when the fibers were failing. That is, the load for the first fiber fracture and the initial crack length were used in equation (17) to determine K. Subsequent rows of fiber fracture allowed K to be calculated from the appropriate load and crack length represented by the initial crack plus the number of inter-fiber spacings over which the crack had traveled. This permitted an average load and hence an average stress intensity factor to be associated with fiber fracture. For example, in one specimen with a volume fraction of 0.10, K ranged from 249 to 303 $kg/mm^{3/2}$ for fiber fracture.

---

† Testing of aluminum-boron composites is in the initial stages and is not reported except for this one result which is for comparative purposes.

Similar calculations for 0.05 and 0.20 volume fraction composites were made, all of the results being given in table I. It is seen that the stress intensity for fiber fracture increases with volume fraction. In fact, K is nearly proportional to $(V_f)^{1/2}$ which has a theoretical basis as discussed below.

Microscopic Observations

Examples of fractures are shown for three different volume fractions in fig. 8. It was observed that the crack would progress in the matrix; a fiber would fracture; the matrix would crack again and then another fiber would fracture. Although it is not obvious in the micrographs, there is a crack in the matrix between the 1st and 2nd fibers for the 0.05 volume fraction; between the 3rd and 4th fibers for the 0.10 volume fraction; and between the 1st and 2nd fibers for the 0.20 volume fraction specimens. Thus, it was assumed that as the crack arrived at the matrix fiber interface, the fracture of the fiber necessitated the fracture strain to be exceeded over the entire fiber diameter. Since the fibers necked considerably before the fracture, the average neck diameter was taken as the value of ℓ^* over which the fracture strain had to be exceeded, as was depicted in fig. 1. The value of ℓ^* was measured from the photomicrographs and is given in table I for each volume fraction.

From the micrographs, the true fracture strain was also measured, the values as determined from equation (18) being given in table I. Although there may be some variation with volume fraction, the average fracture strain of 0.93 for 21 fibers reasonably describes most of the data. To further verify the fracture strain, scanning microscopy gave additional results on 7 fibers, a typical micrograph being shown in fig. 9.

The fracture strain was determined to range from 0.60 to 1.05 with the average being 0.84 for this 0.20 volume fraction specimen. As this is in good agreement with the average value of 0.77 for 0.20 volume fraction data taken from table I, it may be assumed that the rest of the observations are reasonably accurate. Nevertheless, it would appear that there is a statistical variation of about a factor of two in the observed fracture strains.

Fracture Criteria

In the theoretical development, two fracture criteria are suggested for ductile fracture, a crack-tip displacement concept and a critical fracture strain concept. Consider first the fracture strain criterion. Values of ε^* may be calculated from equation (16) from the observed value of K for fiber fracture as taken from the SWE data, and the experimental values for σ_{ys}, E and ℓ^*. From the data in table I, calculated values of ε^* are shown to agree approximately with measured values of ε_f in table II. It should be noted that in this calculation the value for E used in equation (16) was the secondary modulus of elasticity, E_c', which is the appropriate value for a two-phase system wherein the fiber is elastic and the matrix is yielding at the "apparent" elastic-plastic boundary. Rice [20] has shown that in the small volume of material adjacent to the crack, the fracture criterion is dependent upon the unloading path. With these composites, the unloading path would actually be dependent upon both E_c and E_c' but the predominant term is E_c'. Moreover, in a separate study [21], the value of E_c' was successfully utilized to predict the displacement distribution and the critical stress intensity factor in these composites.

Next, consider a critical displacement criterion. Calculating $2v_c^*$

from equation (9) and (15a) is accomplished utilizing the values of K, σ_{ys} and E_c' from table I. This gives a nearly constant value of $2v_c^*$ for all volume fractions and so it would appear that this is just as realistic a criterion as the fracture strain concept. This suggests that these two criteria may be equivalent. In fact, if one combines equations (9), (15a) and (16), this leads to

$$2v_c^* = \pi \ell^* \varepsilon^* \tag{21}$$

which indicates that the critical crack-tip displacement is made up of a microstructural size parameter and a microstructural fracture strain. Using the observed values of ℓ^* and ε_f from table I, an "observed" critical crack-tip displacement is determined from equation (21). In table II, this is seen to be in reasonable agreement with the calculated value of $2v_c^*$. Considering both criteria, there is little to choose between them since the statistical variation in the fracture strain is greater than any differences between observation and calculation. Even though one criterion might be as valid as the other, on pedagogical grounds alone, it seems preferable to lean to the critical fracture strain approach. That is, in less well-defined microstructures, the same critical crack-tip displacement could be made up of a large strain and a small structural size or a small strain and a large structural size. Thus, the flexibility of the two-parameter approach may be necessary to adequately describe the details of the fracture process.

Further substantiation of the overall approach was obtained where it was found [21] that the fiber contribution to the energy dissipation during fracture could be described by

$$G = 2d\, \varepsilon^* \sigma_f V_f \tag{22}$$

Here, 2d is the plastic strip height, which in this case happened to be about twice the fiber diameter. It may be shown that this is essentially equivalent to Rice's "plastic strip" model which is discussed in the Appendix. From equations (15a) and (22), it is seen that the stress intensity for crack propagation would be proportional to $(V_f)^{1/2}$ as long as the plastic strip was independent of the volume fraction. The data in Table I approximately substantiate this relationship. Furthermore, since the product of the strain and plastic strip is approximately $2v_c$, then

$$G = 2v_c\sigma_f V_f \tag{23}$$

which is essentially equation (12b) considering a bulk material where the volume fraction is unity. To demonstrate this equivalence on experimental grounds, the average measured strain of 0.93 times 2d is equal to 0.43 mm. while the average calculated value of $2v_c$ from Table II is 0.52 mm. It should be pointed out that the plastic strip was actually found to be somewhat greater than 2d [21]. This, in conjunction with the fact that the average strain in the plastic strip would be somewhat less than ε_f, probably indicates why $2d\varepsilon^*$ gives a reasonable estimate of the crack-tip displacement.† In summary, it appears that both displacement and fracture strain criteria are valid ductile fracture concepts as substantiated by fracture observations in a two-phase, ductile-fibrous composite. Additional experimental studies involving wide variations in volume fraction, shape, size and fracture ductility of second phases must be run to enable further development of ductile fracture criteria.

---

†It is emphasized that for some other fracture strain, such an agreement between the plastic strip and the fiber diameter would not necessarily be obtained. In fact, for a perfect agreement between equations (22) and (23), it is necessary for $\pi\ell^* = 2d$, which only occurs when $\varepsilon^* = 0.90$, which happens to be the case here. Still, the analysis represented by equation (22) is valid for any fracture strain as long as the plastic strip height is properly assessed.

5. CONCLUSIONS

1. A review of several fracture concepts indicates that both a single-parameter approach, utilizing a critical crack-tip displacement, $2v_c^*$, and a dual-parameter approach, utilizing a structural size factor, ℓ^*, and a critical fracture strain, ε^*, describe ductile fracture at a crack tip.

2. In an aluminum-matrix composite reinforced with unidirectional stainless-steel fibers, both of these models may be utilized as a fracture criterion to predict the critical displacement and/or fracture strain involved in fiber fracture at the crack tip.

3. The statistical variation in the observed fracture strain of the fibers was greater than any differences between observation and theory.

4. Both theoretically and experimentally, it is shown that these two approaches are essentially equivalent since the critical crack-tip displacement contains the other two parameters, i.e.

$$2v_c^* = \pi \ell^* \varepsilon^*$$

Nevertheless, the greater flexibility of the two-parameter approach is to be preferred for the description of the actual fracture process.

5. It is demonstrated that an acoustic emission technique may be utilized to establish the point at which fiber fractures occur during the evaluation of a composite material.

6. If a composite material, with ductile unidirectional fibers, can be approximated by a "plastic-strip" model, then the stress intensity for crack propagation is proportioned to $(V_f)^{1/2}$, V_f being the volume fraction of fibers.

ACKNOWLEDGEMENTS

The author would like to express his appreciation to Professor V. F. Zackay for helpful suggestions on the manuscript and to Dr. D. Porter for the scanning electron microscopy.

This work was supported by the United States Atomic Energy Commission.

TABLE I. Observed Fracture Parameters

Volume Fraction V_f	Stress Intensity[a] K, $Kg/mm^{3/2}$	No. of fibers in estimate	Yield Strength σ_{ys}, Kg/mm^2	Secondary Modulus E'_c, $Kg/mm^2 \times 10^{-3}$	Critical Distance ℓ^*, mm	Fracture Strains, ε_f[b]	
						Range	Average
0.05	196	3	52.5	1.19	.104	(1.45-1.58)	1.52
0.10	262	7	69.6	2.58	.157	(0.37-1.18)	0.72
0.10	289	8	69.6	2.58	.145	(0.69-1.16)	0.94
0.20	518	2	93.0	4.66	.145	(0.86-0.96)	0.91
0.20	434	1	93.0	4.66	.173	(0.55)	0.55

(a) Average value for which fiber fractures were observed.

(b) Measured from diameters in micrographs using Eq. (18).

UCRL-19086 Rev.

TABLE II. Calculated and Observed Fracture Criteria

Volume Fraction V_f	Fracture Strain		Critical Crack-Tip Displacement	
	Calculated ε^*	Observed ε_f	Calculated (a) $2v_c^*$, mm	Observed (b) $2v_c^*=\pi\ell^*\varepsilon_f$, mm
0.05	1.87	1.52	0.62	0.50
0.10	0.77	0.72	0.38	0.36
0.10	1.01	0.94	0.47	0.43
0.20	1.30	0.91	0.60	0.41
0.20	0.80	0.55	0.43	0.30
Average	1.15	0.93	0.50	0.40

(a) $2v_c^* = \frac{K^2}{\sigma_{ys} E}$ (combining equations (9) and (15a))

(b) $2v_c^* = \pi\ell^*\varepsilon^*$ (equation (21))

REFERENCES

1. A. H. Cottrell, "The Tewksbury Symposium on Fracture", C. J. Osborn (editor),(Brown, Prior and Anderson, Ltd., 1965) p. 1.
2. A. A. Wells, British Weld. J., 10 (1963) p. 563.
3. A. S. Tetelman and A. J. McEvily, "Fracture of Structural Materials", (John Wiley and Sons, Inc. New York 1967).
4. F. A. McClintock, Proc. Royal Soc., 285 (1965) p. 58.
5. F. A. McClintock, S. M. Kaplan and C. A. Berg, Jr., Int. J. Fracture Mech., 2 (1966) p. 614.
6. A. A. Griffith, Phil. Trans. Roy. Soc. London, Ser. A 221 (1921) p. 163.
7. "Fracture, Microscopic and Macroscopic Fundamentals", Vol. 1, H. Liebowitz (editor), (Academic Press, Inc., New York 1968).
8. A. Tetelman and T. Johnston, Phil. Mag., 11 (1965) p. 389.
9. E. Orowan, Trans. Inst. Eng. Shipbuild., Scotland, 89 (1945) p. 165.
10. G. R. Irwin, "Fracturing of Metals", Am. Soc. for Metals, Cleveland (1948) p. 149.
11. B. A. Bilby, A. H. Cottrell and K. H. Swinden, Proc. Roy. Soc. London, Ser. A 272 (1963) p. 304.
12. F. A. McClintock and G. R. Irwin, "Fracture Toughness Testing and Its Applications", ASTM STP 381, (Am. Soc. for Test. and Mat'ls., Philadelphia, 1965) p. 84.
13. W. W. Gerberich, "Experimental Mechanics", November (1964) p. 335.
14. F. A. McClintock, ASTM Bulletin, April (1961) p. 277.
15. J. E. Srawley and B. Gross, Materials Res. and Stnds., 7 April (1967) p. 155.

16. V. F. Zackay, W. W. Gerberich and E. R. Parker, "Fracture", Vol. 1, H. Liebowitz (editor), (Academic Press, New York 1968) p. 395.

17. W. W. Gerberich and C. E. Hartbower, "Fundamental Aspects of Stress Corrosion Cracking", R. Staehle (editor), (National Assoc. of Corrosion Eng., Houston 1969) p. 420.

18. W. W. Gerberich, C. E. Hartbower and P. P. Crimmins, Weld. J. Res. Supp., 47 No. 10 (1968) p. 433S.

19. "Aerospace Structural Metals Handbook", Vol. IIA, V. Weiss and J. G. Sessler (editors), (Syracuse University Press, 1966) p. 3203-11.

20. J. R. Rice, Proceedings of the First International Conf. on Fracture, Yokobori, Kawasaki and Swedlow (editors), (Japanese Soc. for Strength and Fracture of Mat'ls, 1966) p. 309.

21. W. W. Gerberich, Fracture in Metal-Metal Composites; Composite Materials Fundamentals and Utilization, University of California, Berkeley, June (1968).

APPENDIX

Rice's [20] plastic strip model essentially simplifies the behavior of real materials to one of a plastically-deforming strip of height, h, being pulled by two elastic slabs. Thus, as the crack propagates in the strip, only the strip deforms and the plastic zone is independent of crack length. Actually, this may approximate some real situations where, as the crack grows by a tearing action, the load drops so that a relatively constant stress intensity is maintained. The strip model may then be used to determine the plastic energy dissipation rate as the plastic deformation extends from $x = \ell + w$ by

$$\gamma_p = h \int_{\ell}^{\ell+w} \sigma_y \frac{\partial \varepsilon_y^p}{\partial \ell} \, dx \qquad \text{(A-1)}$$

with σ_y being the stress and ε_y^p the plastic strain in the strip. If ε_y^p is only a function of the distance from the crack tip $(x - \ell)$, then $\frac{\partial \varepsilon_y^p}{\partial x} = - \frac{\partial \varepsilon_y^p}{\partial \ell}$ and therefore from A-1,

$$\gamma_p = h \int_{x=\ell+w}^{x=\ell} \sigma_y \, d\varepsilon_y^p \qquad \text{(A-2)}$$

Thus, the plastic energy dissipation rate is given by the plastic strip height times the plastic strain energy density within the strip.

LIST OF SYMBOLS

A_o, A_f	Initial, final cross-sectional areas.
a_o	Atomic spacing
B	Specimen thickness
C	Half-crack length
d	Fiber diameter
E	Young's modulus
E_c	Modulus of elasticity of composite
E'_c	Secondary modulus of elasticity of composite
ε	Strain adjacent to crack tip
ε^*	Fracture strain at crack tip
ε_f	Measured fracture strain
ξ_y	Elastic shear strain
ξ^*	Shear fracture strain at crack tip
γ	Work of fracture per unit fracture area
γ_s	Surface tension
γ_p	Plastic energy dissipation per unit fracture area
γ_m	Effective energy absorption per unit fracture area = $\gamma_s + \gamma_p$
G	Strain energy release rate = $2\gamma_m$
$G_{I, III}$	G value appropriate to mode I, III
$K_{I, III}$	Stress intensity factors appropriate to mode I, III
G_{Ic}, G_{IIIc}, K_{Ic}, K_{IIIc}	Critical values at fracture
ℓ	Distance in front of crack

LIST OF SYMBOLS (continued)

ℓ^*	Microstructural unit over which facture occurs
P	Externally applied load
ρ	Crack-tip radius
R_p	Plastic zone diameter
σ	Externally applied stress
σ_c	Theoretical strength of a solid
σ_{comp}	Ultimate strength of a composite
$\sigma_{\{m,\ f\}}$	Subscripts denoting matrix or fiber
σ_{ys}	Uniaxial yield strength
τ_{ys}	Shear yield strength
U	Change of strain energy in a system with a flaw
μ	Shear modulus
V	Potential energy of creating fracture surface
$V_{\{m,\ f\}}$	Volume fraction of matrix or fibers
v	Displacement
v_c	Crack-tip displacement
v_{c^*}	Critical crack-tip displacement at fracture
ν	Poisson's ratio
W	Specimen width

LIST OF FIGURES

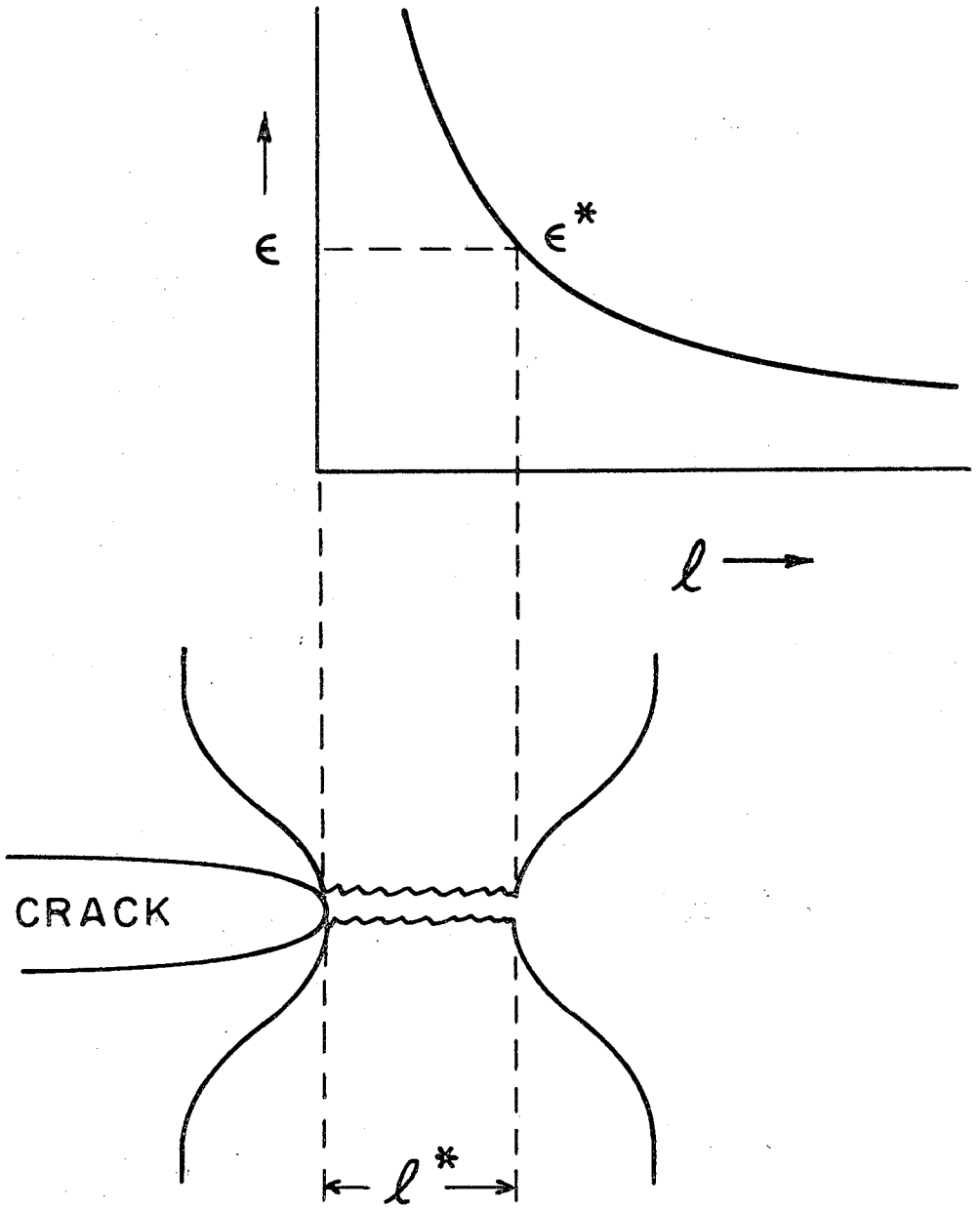

XBL 686-953

Fig. 1

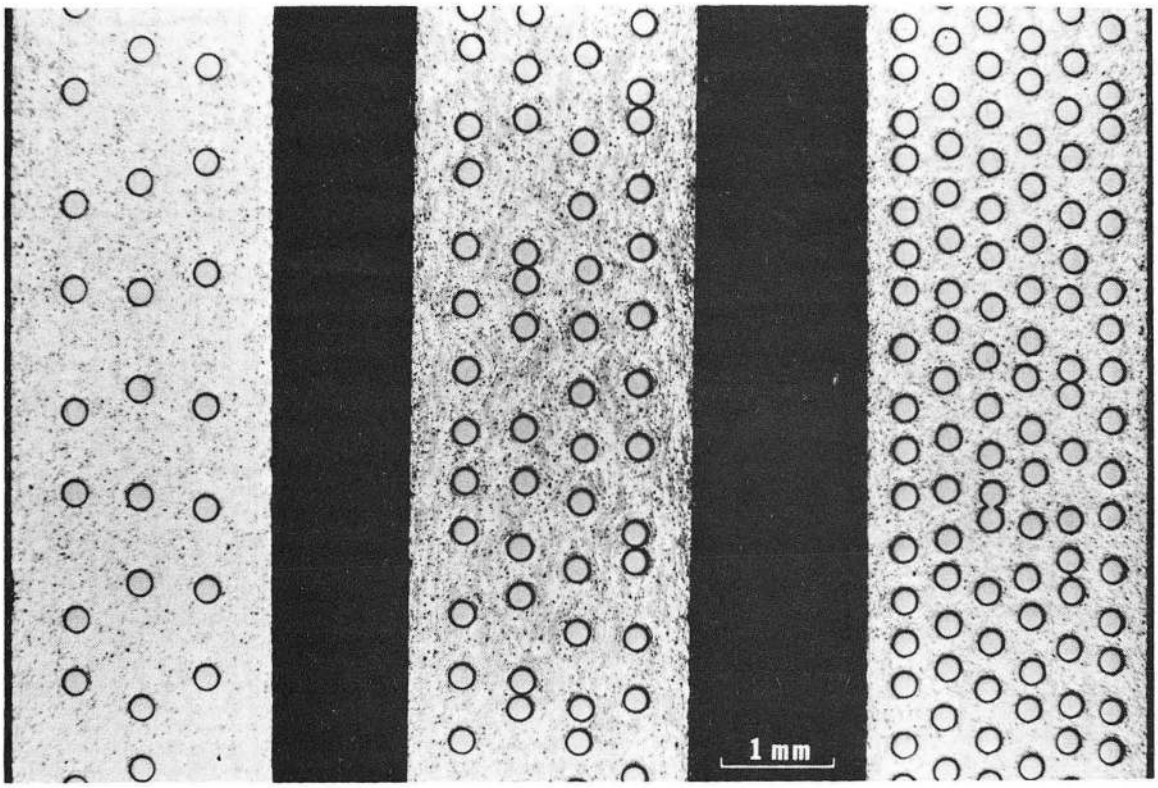

XBB 686-3412-A

Fig. 2

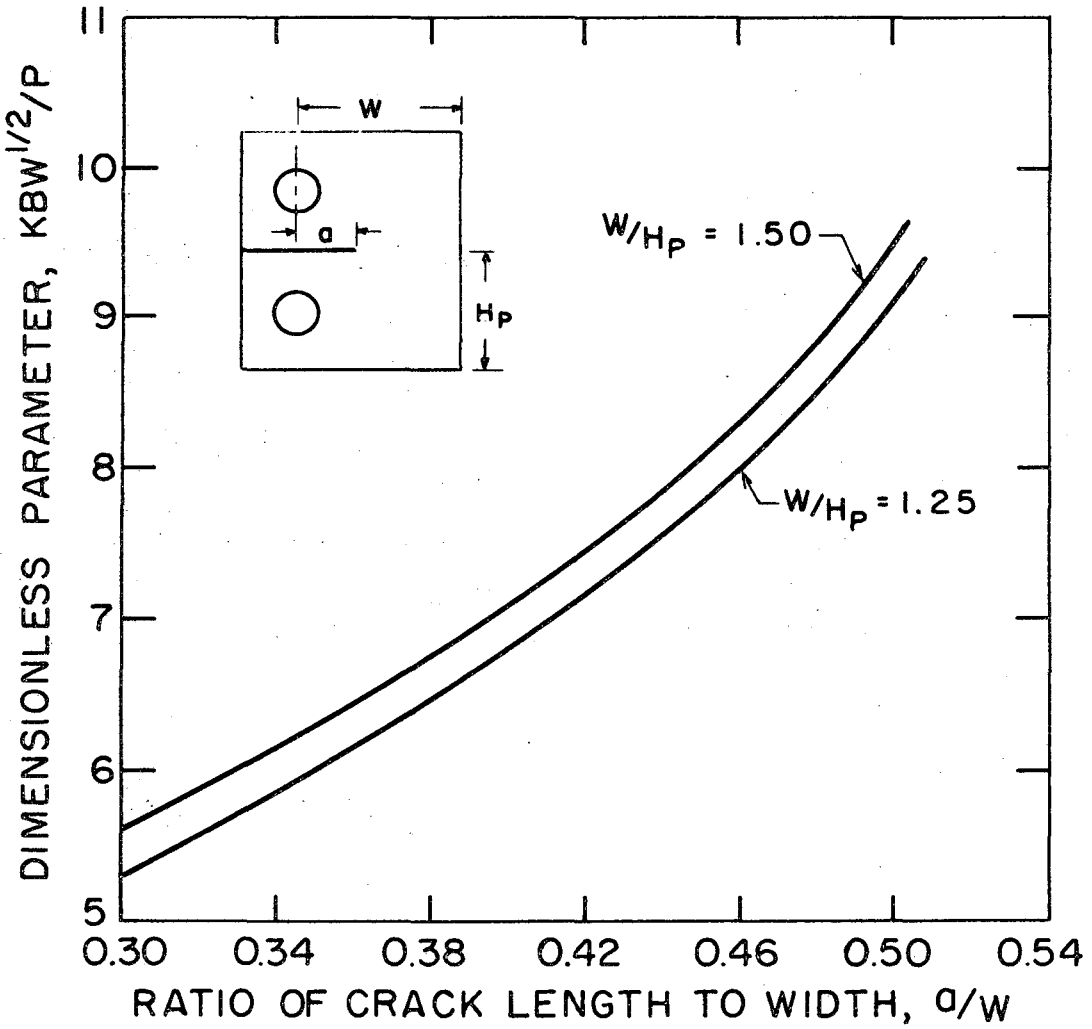

XBL 686-963

Fig. 3

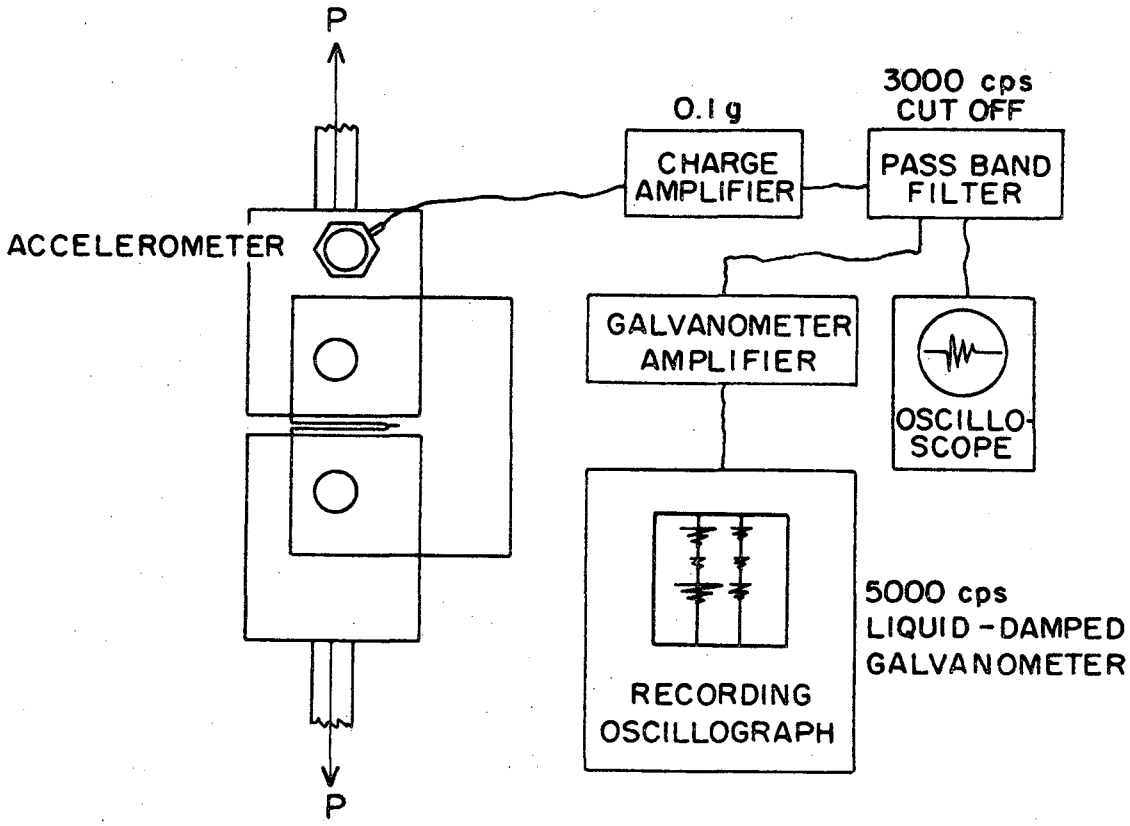

XBL 6812-6412

Fig. 4

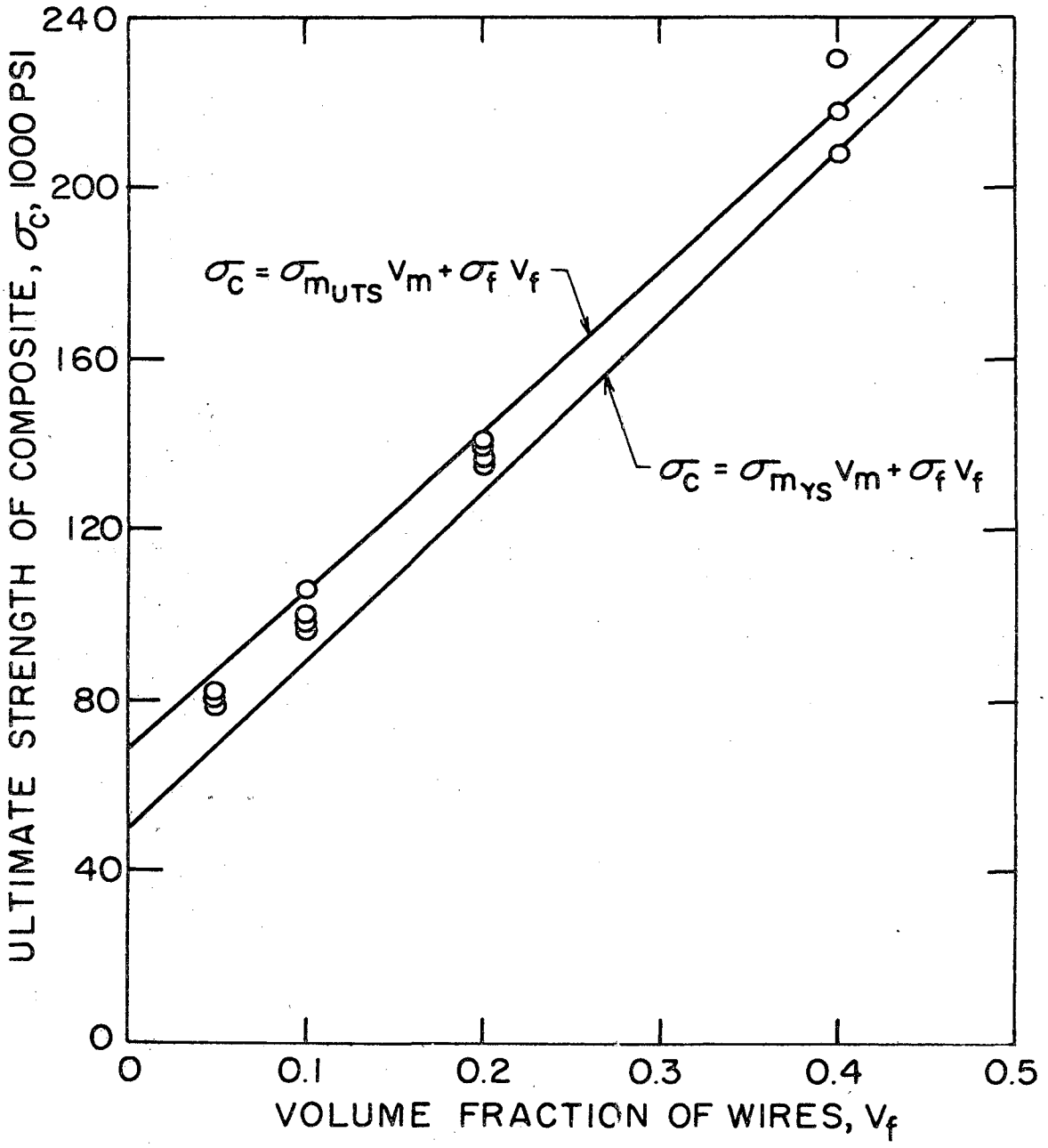

XBL 686-952-A

Fig. 5

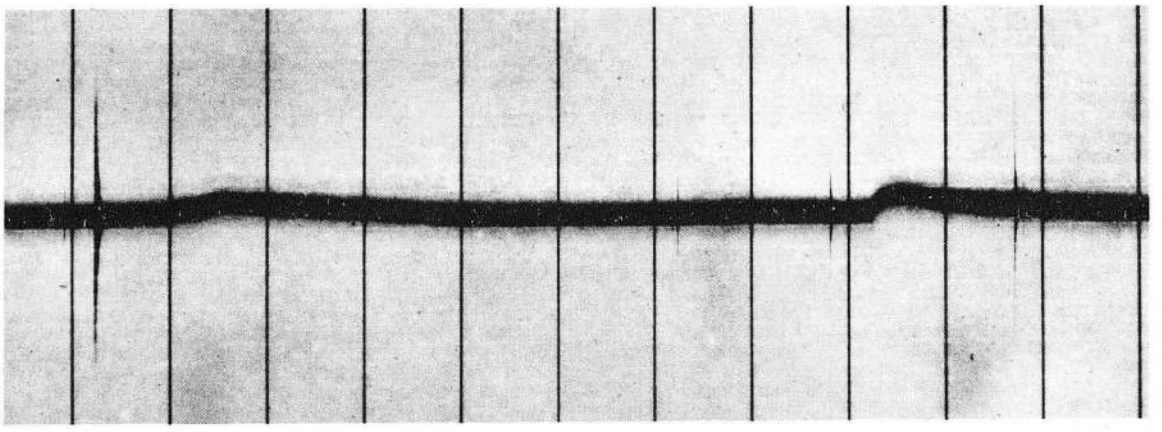

(a) SWE FROM STEEL WIRES 1 SECOND/DIVISION

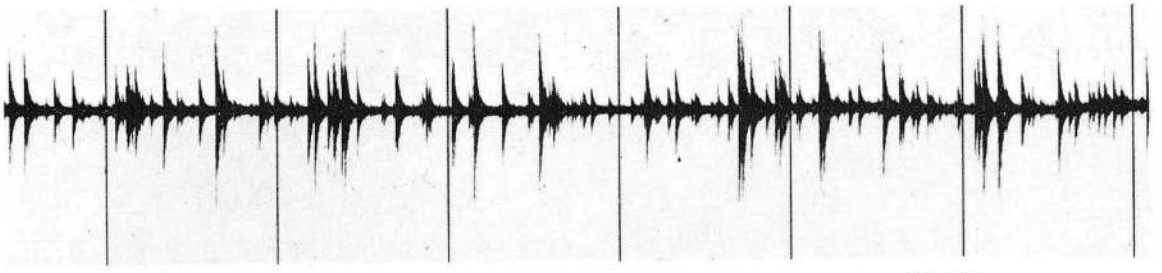

(b) SWE FROM BORON FIBERS 1 SECOND/DIVISION

XBB 6812-7644

Fig. 6

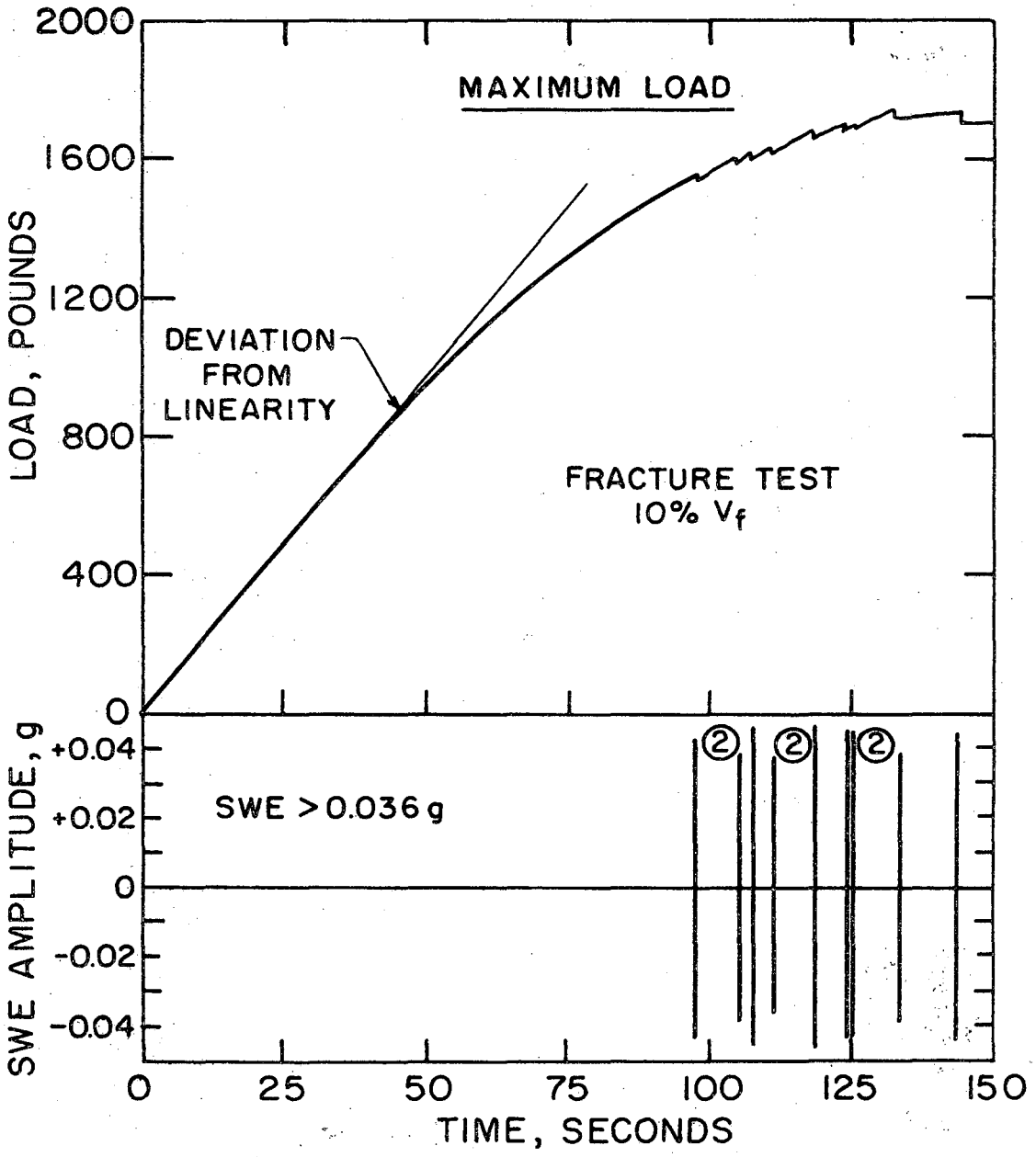

Fig. 7

XBL 686-967

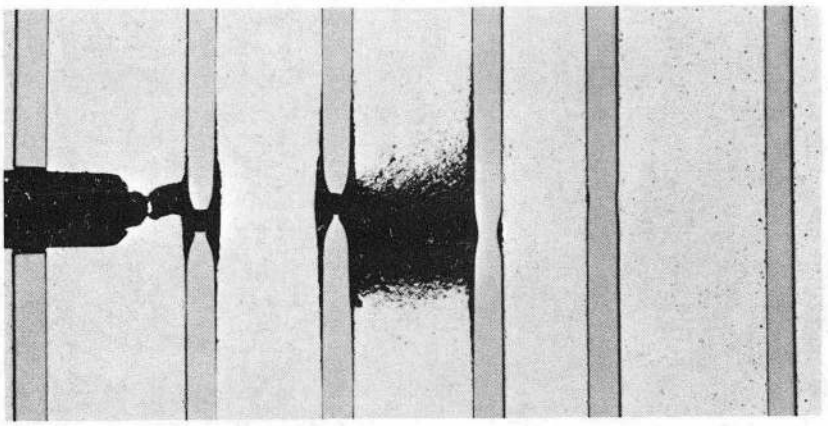

$V_f = 0.05$

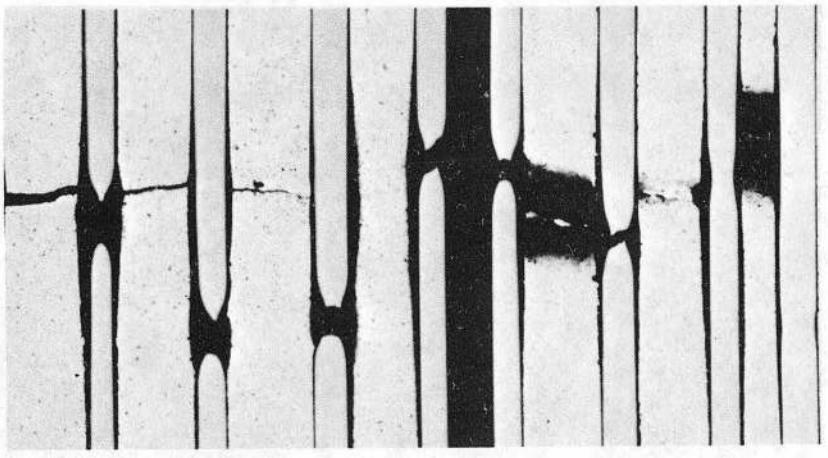

$V_f = 0.10$

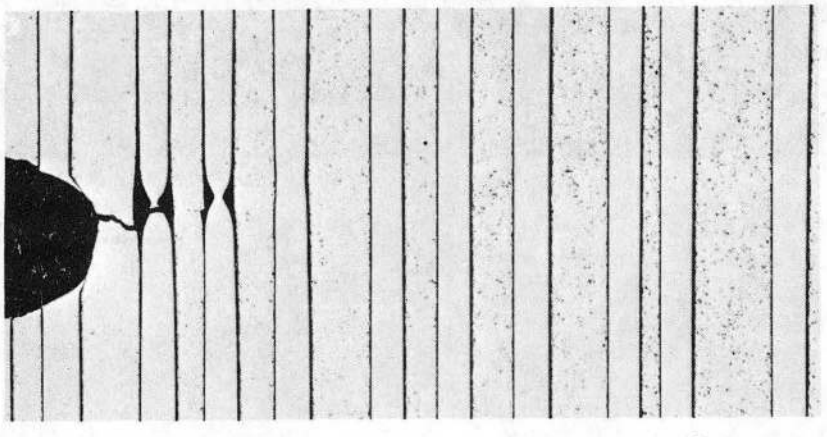

$V_f = 0.20$

1 mm

XBB 686-3411-A

Fig. 8

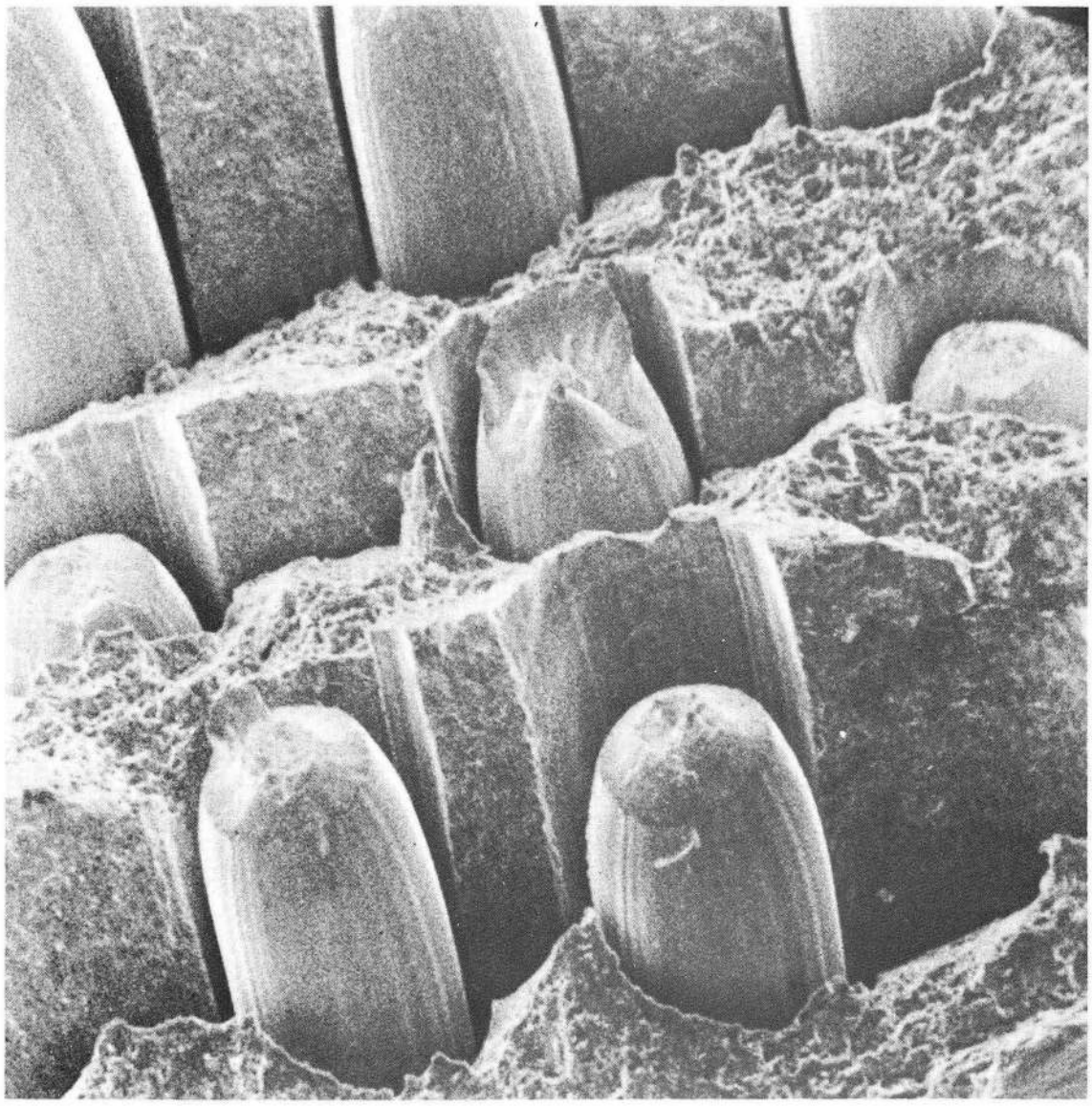

XBB 699-5982

Fig. 9

LEGAL NOTICE